

Space-Charge Limited Schottky Diodes with Wide-Bandgap Thin-film Oxide Heterojunctions

Jihun Lim^{1,2,3*}

¹School of Semiconductor and Chemical Engineering, Jeonbuk National University,
Jeonju, 54896 Republic of Korea

²Department of Department of Semiconductor Science and Technology, Jeonbuk National
University, Jeonju, 54896 Republic of Korea

³Department of Electrical and Computer Engineering, University of Michigan, MI 48109,
USA

*Jihun Lim **email:** jihunlim@jbnu.ac.kr

Keywords: Wide bandgap oxide semiconductor, Thin-film Schottky diode, Breakdown voltage,
Space charge capacitance

Abstract

Non-crystalline thin-film Schottky diodes are cost-effective but often exhibit unreliable electrical characteristics due to material imperfections. In this work, I present a Schottky diode structure utilizing in-situ grown Ta₂O₅ and ZnO thin films deposited at room temperature. The low conduction band offset across the interface of the heterogeneous oxides facilitates efficient electron injection under forward bias. Capacitance-voltage characterization reveals a robust Schottky barrier at the Au/Ta₂O₅ interface without a significant barrier thinning effect, enabling high-voltage breakdown up to 65V and a high on/off ratio of 1×10^8 . In demonstrations, the thin-film structure shows Schottky contact characteristics using even a relatively low work

function metal of ITO, allowing the operation of transparent Schottky diodes. The diodes show additional potential for applications, including RF-to-DC conversion leveraging space charge capacitance at the Ta₂O₅/ZnO junction and rectifying resistive random access memory devices. This work highlights a promising approach for integrating low-cost, high-reliability Schottky diodes into back-end-of-line processes for wireless electronics and power devices.

Introduction

Schottky diodes are fundamental rectifying components used in diverse applications, including automobile electronics,^{1, 2} battery chargers,³ and telecommunications.⁴ High blocking voltage operations and reliability often necessitate the use of expensive materials such as GaN,⁵ SiC,³ and Ga₂O₃^{1, 2, 6}, which have wide bandgaps and high crystallinity. However, these materials present challenges due to their high cost, limited scalability, and complex manufacturing processes, which can hinder their integration into advanced, cost-effective electronics. To address these issues, researchers have explored the use of thin-film materials, such as oxide semiconductors,^{7, 8} graphene,⁹⁻¹¹ and transition metal dichalcogenides (TMDs),^{1, 9, 12}. TMDs are particularly attractive due to their potential to form defect-free metal-to-semiconductor junctions, which can achieve nearly ideal Schottky barriers and enable reliable rectification. Graphene, with its tunable work functions and van der Waals heterostructures, has improved the formation of Schottky junctions with Si or TMDs.^{9, 10, 13} However, the challenges remain with graphene and TMDs, including difficulties in achieving high-quality large-scale production, precise control of film thicknesses, and compatibility with existing semiconductor processes, which raises questions about their commercialization prospects.

In contrast, oxide materials such as Indium–gallium–zinc–oxide (IGZO) and zinc oxide (ZnO) have demonstrated flexible Schottky diodes with gigahertz cutoff frequencies (f_c).^{7, 8}

Especially, due to their compatibility with existing manufacturing processes, the materials support conventional mass productions in display markets.¹⁴ However, oxide thin-film devices often deviate from the Schottky-Mott rule due to junction defects and Fermi-level pinning effect, which can result in relatively high reverse currents and low breakdown voltages.^{10, 15}

In this study, I introduce Ta₂O₅/ZnO heterostructure generated through in-situ rf-sputtering deposition at room temperature. A Schottky barrier is formed at the interface between Au and Ta₂O₅, which is not suffered from barrier thinning effects and allows for high blocking voltages up to 65V. Under forward bias, the low conduction band offset at the Ta₂O₅/ZnO junction enables electron injection from ZnO to Ta₂O₅. The voltage primarily drops across Ta₂O₅, where the drift mechanism governs charge transport to the Au electrode. At the Ta₂O₅/ZnO interface, electrons accumulate and diffuse to the Au, resulting in space-charge limited current (SCLC) characteristics. By replacing Au with ITO, an all-oxide Schottky diode is demonstrated on glass substrates, with an average transmittance of approximately 80 % in visible wavelengths. The addition of a thin 5-nm-thick TaO_x layer between Ta₂O₅ and ZnO creates both trap-filled and trap-free SCLC regimes, resulting in a resistive random-access memory (ReRAM) function with high resistance window exceeding 10⁴. Thus, the Schottky diode structure offers potential applications in low-cost, high-yield Schottky diodes, transparent electronics, and advanced memories.

Experimental Section

Device Fabrication

To prepare a thin-film Ta₂O₅/ZnO Schottky diode, a 10-nm-thick Ti adhesion layer and a 100-nm-thick Au layer are sequentially deposited by sputtering onto a cleaned glass substrate.

The mesa structure of Ta₂O₅/ZnO double layers is then patterned using standard lift-off processes, followed by in-situ rf-magnetron sputtering deposition of Ta₂O₅ and ZnO targets (Kult J. Lesker) of 99.999% purity. A 100-nm ITO top-electrode is deposited by sputtering and patterned using liftoff processes. For an all-oxide transparent Schottky diode, the same processes are used, but the bottom electrode is replaced with ITO deposited by dc sputtering. To prepare a crossbar Schottky diode, a 10-nm-thick Ir and a 50-nm-thick Au layers are sequentially deposited by sputtering onto a cleaned glass substrate and patterned using standard liftoff processes. Four layers – Ta₂O₅ (200nm), TaO_x (5nm), ZnO (50nm), and ITO (50nm) – are then deposited by in-situ sputtering and patterned using standard liftoff processes. The TaO_x is deposited by reactive dc magnetron sputtering in a mixed atmosphere of Ar (10 sccm) and O₂ (30 sccm) pressures.

Measurements

The current-voltage and capacitance-voltage characteristics were measured using a Keithley 4200 semiconductor analyzer with source-measure units and capacitance-measure units. For half-wave rectification measurements, a waveform generator (Agilent 33220A) provided sine-wave input voltage to the diode, and the output voltage is recorded with an oscilloscope (Agilent DSO7054A). The transmittance of all-oxide Schottky diodes is measured using a spectroscopic ellipsometer (J.A. Woollam M-2000).

Results and Discussion

Characterization of Ta₂O₅/ZnO Hetero-oxide Schottky Diode

Figure 1a illustrates the energy band structure of the Ta₂O₅/ZnO heterojunction. The Schottky barrier (ϕ_b) is formed at the metal/Ta₂O₅ interface. According to the Schottky-Mott

rule, ideal ϕ_b can range from 1.2 eV to 0.7 eV, depending on the work functions of metals. Figure 1b indicates the measurement using the Schottky diode. The ITO is grounded while the voltage is applied to the Au. The symbols represent the measured data using the diode, with the red solid lines indicating the SCLC characteristics following the relationship $J \propto V^2$ according to the Mott-Guttley law¹⁶, influenced by the band offset and charge accumulation. The inset shows an optical image of the diode with the Au and ITO contacts at the bottom and top, respectively. It retains an on/off ratio of higher than 10^6 .

Figure 1c shows the current-voltage characteristics of Au/Ta₂O₅/ITO and Au/ZnO/ITO devices. The Ta₂O₅ device has a Fermi level close to the conduction band,¹⁷ and exhibits diode behavior with bi-Schottky barriers at the Au and ITO contacts. Due to the relatively high work function of Au compared to ITO, the turn-on voltage (V_T) at forward bias is smaller than at reverse bias. A typical Au/ZnO device with low defects can show Schottky diode behavior¹⁸, but the experiment shows ohmic behavior due to high defects in the ZnO layer.¹⁹ Figure S1 shows the photoluminescence measurements of two different ZnO thin films on glass substrates, prepared by sputtering at room temperature and atomic layer deposition at 150 °C, respectively. By inserting the Ta₂O₅ between the Au and sputtering-ZnO layers, the ZnO acts as the electron transport layer to the Ta₂O₅ layer.

The reciprocal capacitance-voltage characteristics is investigated to estimate the built-in potential (ϕ_{bi}) in the Schottky-diode structure. Figure 1d shows the equivalent circuit of the Schottky diode. The C_f means free charges of electrons, C_L is the localized trapped charges due to imperfect materials, and R_L is the resistance responding to a given voltage by the trapped charges. From the imaginary impedance of the circuit (see the full derivation in Note 1, Supporting Information), the frequency-dependent capacitance is expressed by:

$$C(\omega) = \frac{(C_L + C_f)^2 + \omega^2 R_L^2 C_L^2 C_f^2}{(C_L + C_f) + \omega^2 R_L^2 C_L^2 C_f}, \quad (1)$$

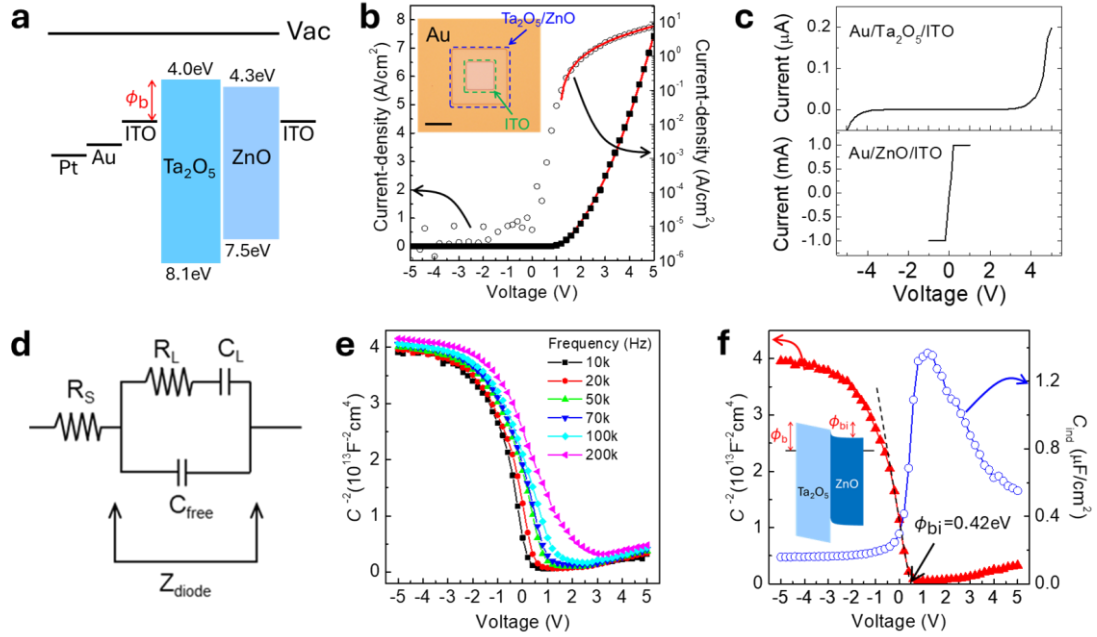


Figure 1. The characterization of the Ta₂O₅/ZnO hetero-oxide diode. a) Band diagram of the Ta₂O₅/ZnO Schottky diode. The ϕ_b indicates the Schottky energy barrier. The hetero-oxide structure is grown by in-situ sputtering at room temperature. b) Current-density versus voltage using the Schottky diode. The left and right y-axis indicate linear and log-scale current densities, respectively. The inset shows an optical microscopy image of the diode. Scale bar, 50 μ m. c) Current-voltage characteristics of Au/Ta₂O₅/ITO (top) and Au/ZnO/ITO (bottom) devices. The current compliance was set to 1mA. d) Equivalent circuit model of the Schottky diode. R_s is the series resistance, R_L is the localized resistance, C_L is the localized capacitance, and C_{free} is the capacitance due to free charges. Z_{diode} indicates the frequency-dependent impedance. e) Reciprocal of the square of capacitance with multi frequencies ranging from 10k Hz to 200k Hz. f) Extracted frequency-independent reciprocal of the square of capacitance (left-y axis) and the capacitance (right-y axis). The ϕ_{bi} is the built-in potential, interpolated from the linear dashed line at $C^{-2} = 0$.

where the three unknowns of C_f , C_L , and R_L are calculated using the three equations for $C(\omega)$.

Figure 1e plots the measured reciprocal of the square of capacitance ($1/C^2$) with multi frequencies from 10 kHz to 200 kHz. The three unknowns are determined by choosing three frequencies (e.g., 20kHz, 100kHz, and 200kHz) from the plots. Then, the frequency-independent capacitance (C_{ind}) is defined by the sum of C_L and C_{free} . Figure 1f represents the C_{ind} , where the built-in potential of 0.42 eV is defined at the interface between Ta₂O₅ and ZnO, as illustrated by the inset.

Details of Band Structures and High Blocking Voltage Capabilities

Figure 2a illustrates the energy-band structures of the Schottky diode under forward and reverse biases. The conduction band offset between Ta₂O₅ and ZnO is about 0.3 eV. A relatively low band offset can facilitate electron injection from ZnO to Ta₂O₅. Due to the offset, electrons accumulate at the Ta₂O₅/ZnO interface under forward bias, creating a space charge region. The electrons injected into the Ta₂O₅ diffuse and drift towards the Au contact due to the electric field within Ta₂O₅ (see Note 2 in Supporting Information). Under forward bias, the voltage is mostly dropped across the Ta₂O₅/ZnO junction and Ta₂O₅. At the junction, the conduction band of the ZnO at bends downward, resulting in the accumulation of electrons. Free electrons (n_{free}), expressed by $n_{\text{free}} = \int_{E_{\text{CBO}}}^{\infty} n_{\text{acc}} dE$ (where E_{CBO} is the conduction band offset at the Ta₂O₅/ZnO interface), are injected from ZnO to Ta₂O₅ and flow through Ta₂O₅ to the Au. This decides the amplitude of the forward current.

Figure 2b shows the reverse current density (J_{rev}) versus voltage up to 65V, measured over 10 cycles. The red dashed line and blue symbol represent the initial and final measurements, respectively. The curve increases slightly during the cycles. The trend is saturated, not significant enough to break down the Schottky barrier. Here the reverse current is determined by three types of charge transport: field emission (J_{FE}), thermionic-field emission (J_{TFE}), and thermionic emission (J_{TE}). J_{TFE} and J_{TE} can be suppressed when the Schottky barrier is relatively high. The room-temperature-grown Ta₂O₅ has defects, which induce charge transport by trap-assisted tunneling, thereby contributing to J_{FE} ²⁰. The reverse current does not exponentially increase, indicating that the barrier thinning effect does not occur in the structure. This is because the electric field is evenly distributed across the 200-nm-thick Ta₂O₅ layer,

mitigating the thinning effect typically observed in thin-film metal-semiconductor Schottky-junctions ⁷.

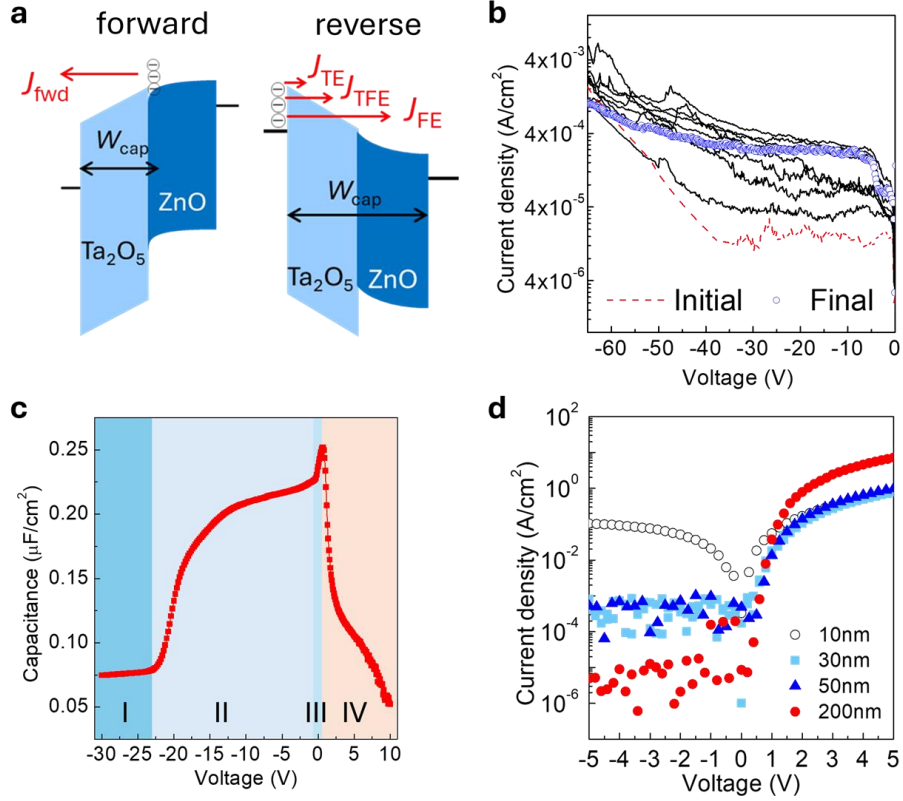


Figure 2. High Blocking Voltage in the Ta₂O₅/ZnO Structure. a) Illustrative band structures of the Ta₂O₅/ZnO Schottky diode under forward and reverse biases. W_{cap} is the capacitance width. J_{fwd} is the forward current density. J_{TE} , J_{TFE} , and J_{FE} are thermionic, thermionic-field emission, and field-emission current densities, respectively. b) Reverse current-density curves during 10 continuous measurements. c) Measurement of capacitance-voltage characteristics using the Schottky diode with four regions. I: Fully depleted Ta₂O₅/ZnO, II: Partially depleted ZnO, III: Charge accumulation at the interface of Ta₂O₅/ZnO, IV: Strong charge accumulation at the interface of Ta₂O₅/ZnO. d) Current-density versus voltage for Ta₂O₅/ZnO Schottky diodes with Ta₂O₅ thicknesses were 10nm, 50nm, 200nm, and 500nm.

Figure 2c presents the capacitance-voltage characterization to aid understanding of the band structure via applied voltages. In the region-I, the curve is nearly flat, indicating fully depleted Ta₂O₅ and ZnO layers. In the region-II, the depleted region in the ZnO decreases as the reverse bias is reduced. At near-zero bias in the region-III, the ZnO is negatively charged due to electrons, which accumulate at the Ta₂O₅/ZnO interface. The capacitance rises to its peak

value, determined by the thickness of the accumulation layer. Figure S2 (Supporting Information) shows the hysteresis measurement in the diode, indicating a small window due to charge trapping. Therefore, although the room-temperature process can introduce defect states at the interface, they can be negligible. In the region-IV, electrons accumulate at the interface and the accumulation depth extends into the ZnO layer, causing the capacitance to decrease again.

Figure 2d shows the comparison of the current-voltage characteristics of Ta₂O₅/ZnO Schottky diodes with different Ta₂O₅ thicknesses ($t_{\text{Ta}_2\text{O}_5}$) of 10nm, 30nm, 50nm, and 200nm. Charges, by a diffusion-drift mechanism (Figure S4 and Note 2 in Supporting Information), flow through Ta₂O₅. The voltage drops (V_{drop}) mainly occur in the Ta₂O₅ layer, indicating that the drift mechanism is dominant in the Ta₂O₅ layer. As $t_{\text{Ta}_2\text{O}_5}$ increases, the reverse current is significantly suppressed due to a relatively long path for charge transport. Numerically, the forward current is expected to be reduced due to the decreased electric field in Ta₂O₅. However, the experiment shows an improvement in the forward current. This is understood by the effect of the rise in substrate temperature during long time rf-magnetron sputtering,²¹ which can lead to a reduction of defects near the Ta₂O₅/ZnO interface, enhancing the charge injection. To validate the analysis of the thickness-dependent trend, Figure S3 provides the statistical analysis of the Schottky diodes with the different Ta₂O₅ thicknesses.

Half-wave Rectification and RF-DC Conversion

Figure 3a shows the schematic of the half-wave rectifier circuit using the Ta₂O₅/ZnO Schottky diode. A plastic-circuit board was used to connect the Schottky diode to a waveform generator, a load resistor (R_L) of 1M Ω , and an oscilloscope (see Experimental section). Figure 3b indicates the half-wave rectification output voltage (V_o) under a 1 Hz sine-wave input (V_{IN})

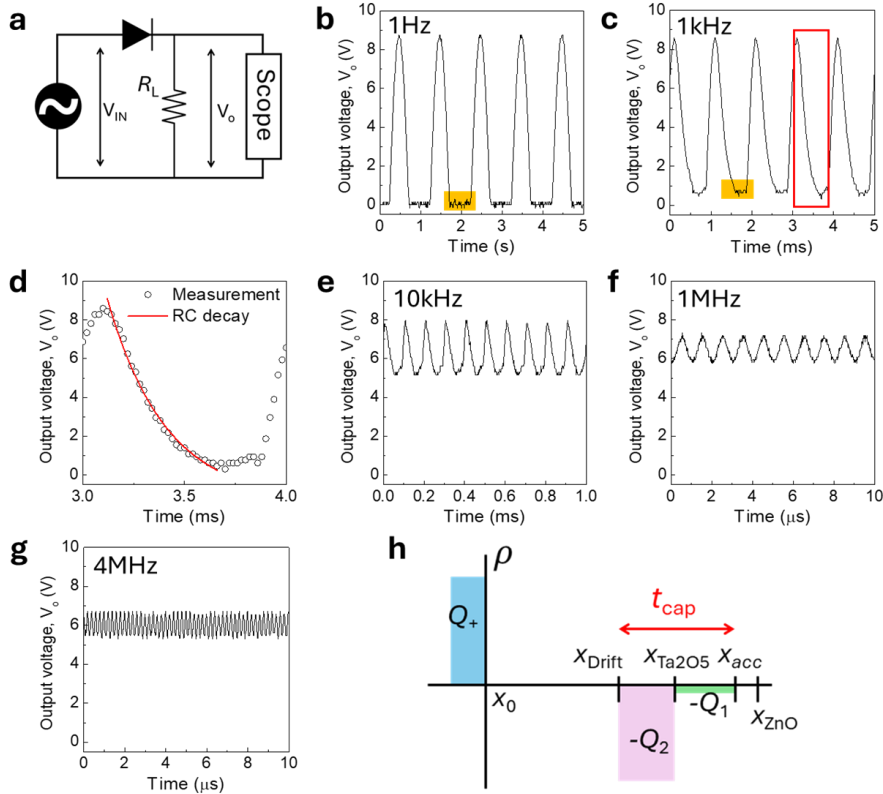


Figure 3. Half-wave Rectification and RF-DC Conversion. a) Schematic of the half-wave rectifier circuit using the Ta₂O₅/ZnO Schottky diode. V_{IN} : Input voltage, R_L : Load resistor, V_o : Output voltage. The experiment setup is described in Experiment section. b) to g) Measured V_o using a sine-wave V_{IN} with varying frequencies. d) shows the extended plot marked by the red box in c). The red solid line is the fitted exponential line due to resistive-capacitive discharging effect. h) Illustration of the charge distribution in the Schottky diode under forward bias. Q_+ represent the positive charge at X_0 . Q_1 denotes the accumulated electron charges at the Ta₂O₅/ZnO interface. Q_2 is the charges in the depleted Ta₂O₅ region. X_0 is the Au/Ta₂O₅ junction, X_{Drift} is the starting point of the drift region in Ta₂O₅, X_{Ta2O5} is the Ta₂O₅/ZnO junction, and X_{acc} is the endpoint of charge accumulation in ZnO.

with a peak-to-peak (V_{p-p}) of 20V. The colored box highlights the rectification of the negative bias region. Figure 3c shows the V_o under a 1kHz sine-wave V_{IN} with the same V_{p-p} , where the colored box indicates that the negative bias is not fully rectified. Figure 3d is an extended graph of the red box in Fig. 3c, showing the decay of discharging due to resistance and capacitance components in the diode structure. The capacitance is determined by Ta₂O₅ and electron accumulation as described in Fig. 2c. The red line represents the fitted resistive-capacitive (RC) accumulation as described in Fig. 2c. The red line represents the fitted resistive-capacitive (RC) delay curve, fitted by the exponential function of $e^{-t/\tau}$ (τ : time constant of 2.86×10^{-4}). By further

increasing the frequency up to 4 MHz, Figures 3e to 3g show that V_o is characterized by direct current (DC) conversion. This is due to the increase in RC delay, as illustrated in Fig. 3h. The RC delay is determined by the charge distribution in the Schottky diode under forward bias. Hole charges are blocked by the Ta_2O_5 , resulting in a positive charge at the metal interface. X_o is the junction between the metal and Ta_2O_5 . The charge Q_1 is formed between $X_{Ta_2O_5}$ and X_{acc} due to electron accumulation. The charge Q_2 between $X_{Ta_2O_5}$ and X_{Drift} is determined by the diffused electrons. The sum of Q_1 and Q_2 equals Q_+ , with Q_1 and Q_2 controlled by material properties such as carrier concentration in ZnO, the E_{CBO} , and the density of defects in Ta_2O_5 . The t_{cap} is the thickness of the junction capacitance generated across the region between X_{Drift} and X_{acc} . A relatively strong field forms from X_{Drift} to X_o , accelerating electrons towards the metal. When the diode is reverse-biased, Q_1 and Q_2 are discharged due to RC delay, which characterizes the radio frequency (RF) to DC conversion observed in Figs. 3e to 3g. A high responsivity is important for RF-to-DC conversion, and Figure S5 and Note 3 (Supporting Information) indicate the estimated responsivity (A/W) in the Schottky diode, which is higher than 20.

All-Oxide Schottky Diode and Rectifying Resistive Memory

Figure 4a shows the rectification current-voltage curve for the all-oxide Schottky diode, illustrated by the inset. The top ITO is grounded while the applied voltage is swept at the bottom ITO. Figure S6 and Note 4 (Supporting Information) show the calculation of the Schottky barrier from the observation of reverse saturation current using the diode. Using Richardson's law, the Schottky barrier at the ITO/ Ta_2O_5 interface is estimated to be about 0.63 eV, which is lower than 1.2 eV barrier at the Au/ Ta_2O_5 interface. The relatively low barrier increases the reverse current due to enhanced electron injection by J_{FE} , J_{TFE} , and J_{TE} . It can compromise

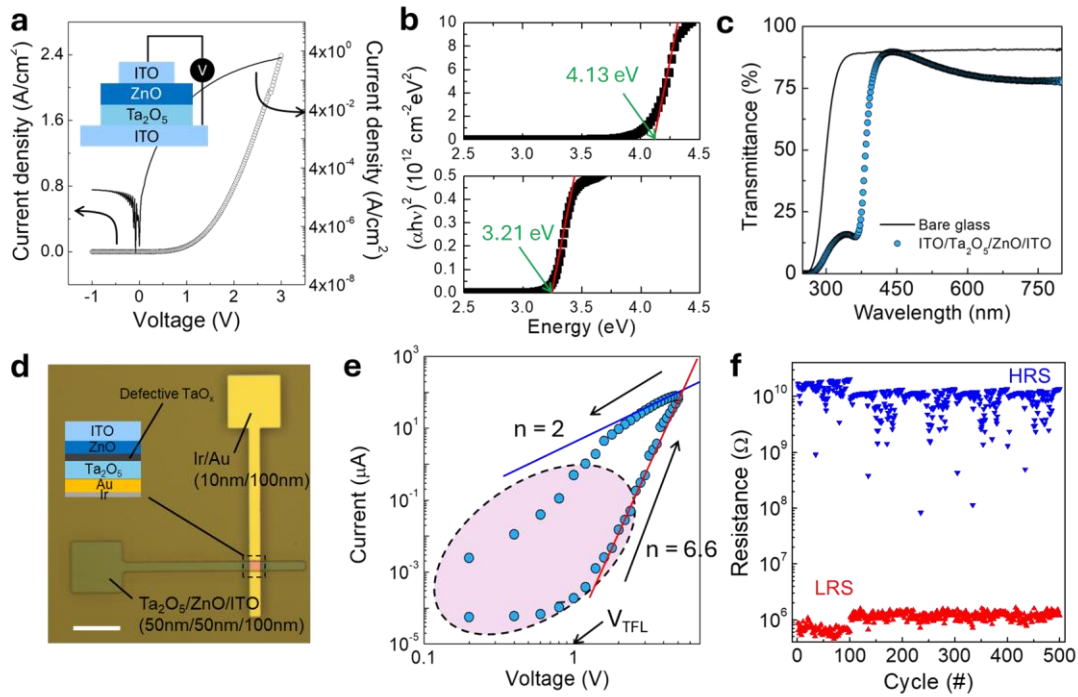


Figure 4. Transparent Schottky Diode and Resistive Memory Structure. a) Current density versus voltage measurement for an all oxide Ta₂O₅/ZnO Schottky diode. The inset shows the schematic of the diode structure. b) Optical bandgap characteristics of Ta₂O₅ (top) and ZnO (bottom) thin films. c) Transmittance of the transparent Schottky diode (symbols). The solid line represents the transmittance of a bare glass substrate. d) Optical microscope image of a crossbar rectifying resistive memory structure. The inset shows the thin film stack of Ir/Au/Ta₂O₅/Ta₂O₅/ZnO/ITO. Scale bar, 50μm. e) Hysteresis characterization using the crossbar device. The dashed ellipse highlights the region associated with charge trapping and detrapping mechanisms. f) Retention test of the memory window between low-resistance state (LRS) and high-resistance state (HRS) over 500 cycles.

relatively high-reverse voltage operation. However, it shows reliable rectification within the reduced voltage range of -1V to 3V. In Fig. 4b, the optical bandgaps for Ta₂O₅ and ZnO are estimated to be 4.13 eV and 3.21 eV, respectively. Figure 4c) shows the measured transmittance using the all-oxide Schottky diode. It exhibits a transmittance of approximately 83.4% in the visible wavelength range of 400nm to 700nm. The demonstration without using pristine metals such as Au and Pt supports its application in inexpensive and transparent electronics, including wearable devices and transparent energy harvesting systems, which require wireless power control units with RF-DC converters.

Figure 4d shows the optical microscope image of a crossbar Schottky diode structure fabricated on a glass substrate. The top metal is grounded while the bottom metal is swept by the applied voltage. The bottom metal consists of double layers of Ir/Au with thicknesses of 10nm/100nm, where Ir serves as the adhesive layer on the glass substrate. During the in-situ deposition of the top thin-film layers, a 5 nm defect-rich TaO_x layer is sandwiched between the Ta₂O₅ and ZnO layers using the reactive sputtering method, where positive oxygen vacancies play a role in trapping electrons²². Figure S7 (Supporting Information) shows the measured transmittance of the TaO_x, which shows optical bandgap narrowing compared to that of Ta₂O₅, implying that TaO_x is defect-rich near the conduction band minimum.²³ The inset illustrates the thin-film stack at the cross region, which has an area of 10μm×10μm. Using the diode, Figure 4e shows the current-voltage hysteresis measurement, demonstrating resistive memory behavior. Figure S8 (Supporting Information) illustrates the mechanism behind the formation of the resistive memory window. At a negative bias, the ionized oxygen defects in the TaO_x layer remain positively charged without significant electron trapping, thereby establishing the interfacial polarization at the TaO_x/ZnO junction. During the voltage ramping up, the shallow defect states are filled by electrons. At a forward voltage less than the trap-filled limit voltage (V_{TFL}) of approximately 1V, the conduction band of the ZnO bends downward at the interface of ZnO/TaO_x, exposing electrons to deep trap states in the TaO_x. When the applied voltage exceeds V_{TFL} , the curve is governed by trap-limited SCLC with the relationship of $I_d \propto V^n$,²⁴ where n is 6.7 during the voltage ramping up. The process of trap filling suppresses the polarization in the Ta₂O₅, and the field across the Ta₂O₅ drives electrons to the Schottky metal contact. As the voltage increases, the trap states are continuously filled, and the polarization switches to the reverse direction. At a relatively high voltage, the traps in the TaO_x can be fully occupied by electrons. Therefore, the TaO_x layer is considered a trap-free interface. At this

stage, the voltage is estimated to be higher than 5V; however, the device was not tested at voltages higher than 5V to prevent breakdown. During voltage ramp-down, the current-voltage curve ($n = 2$) behaves similar to the Ta₂O₅/ZnO Schottky diodes. Below V_{TFL} , the curve deviates from the guideline for $n = 2$ (increasing), indicating that the TaO_x returns to a positively charged state due to charge detrapping. The switch of polarization at the TaO_x interface generates the resistive memory characteristics.

Figure 4f represents the retention test of charge trapping and detrapping processes during hysteresis measurements across 500 consecutive cycles. Figure S9 (Supporting Information) shows the full set of the measurements across the bias range from -5V to +5V. The ratio of the high resistance state (HRS) to low resistance state (LRS) is approximately 10^4 , which is sufficiently high to reflect weight updates determined by conductance changes during the gradient descent optimization method for memory-based machine learning.²⁵ Figure S10 (Supporting Information) shows the optimized bias range to achieve a highest ratio of the HRS to LRS. The reliable switching characteristics suggest that this concept is a suitable candidate for realizing simple crossbar resistive memory chips, not demanding switching components such as transistors.

Conclusion

Room-temperature, in-situ grown Ta₂O₅/ZnO Schottky-diodes are demonstrated, showing their high performance with an on/off ratio higher than 10^8 . A reverse blocking voltage is estimated to be at least 65V. The Schottky barrier at the metal/Ta₂O₅ interface accommodates a wide range of metal work functions from Pt to ITO, enabling the creation of all-oxide Schottky-diodes with over 80% transparency in the visible spectrum. Furthermore, I demonstrate the versatility of these diodes in applications such as half-wave rectifiers, RF-DC

conversion, and crossbar resistive memory, highlighting their current rectification capabilities. The demonstrations present a promising method for integrating the Schottky diodes into the back-end of chips, utilizing low-cost, low-temperature processes and high throughput, which are crucial for reducing environment impact and promoting sustainability.

Acknowledgements

This preprint does not include acknowledgements. Information on financial support and grants will be provided in the final published article.

Author contributions statement

Jihun Lim was responsible for designing the experiments and conducting the sample measurements. In addition, Jihun Lim analyzed the data and prepared and wrote the manuscript.

Data availability statement

The data and materials that support the findings of this study are available from the corresponding author upon reasonable request.

Conflict of Interest

The authors declare no conflict of interest.

Reference

- (1) Yang, S. J.; Park, K.-T.; Im, J.; Hong, S.; Lee, Y.; Min, B.-W.; Kim, K.; Im, S. Ultrafast 27 GHz cutoff frequency in vertical WSe₂ Schottky diodes with extremely low contact resistance. *Nature communications* **2020**, *11* (1), 1574.
- (2) Harada, T.; Ito, S.; Tsukazaki, A. Electric dipole effect in PdCoO₂/β-Ga₂O₃ Schottky diodes for high-temperature operation. *Science advances* **2019**, *5* (10), eaax5733.
- (3) Whitaker, B.; Barkley, A.; Cole, Z.; Passmore, B.; Martin, D.; McNutt, T. R.; Lostetter, A. B.; Lee, J. S.; Shiozaki, K. A high-density, high-efficiency, isolated on-board vehicle battery charger utilizing silicon carbide power devices. *IEEE Transactions on Power Electronics* **2013**, *29* (5), 2606-2617.
- (4) Spiazzi, G.; Buso, S.; Citron, M.; Corradin, M.; Pierobon, R. Performance evaluation of a Schottky SiC power diode in a boost PFC application. *IEEE Transactions on Power Electronics* **2003**, *18* (6), 1249-1253.
- (5) Wang, L.; Nathan, M.; Lim, T. H.; Khan, M. A.; Chen, Q. High barrier height gan schottky diodes: Pt/gan and pd/gan. *Applied Physics Letters* **1996**, *68* (9), 1267-1269.
- (6) Lu, X.; Zhang, X.; Jiang, H.; Zou, X.; Lau, K. M.; Wang, G. Vertical β - Ga₂O₃ Schottky barrier diodes with enhanced breakdown voltage and high switching performance. *physica status solidi (a)* **2020**, *217* (3), 1900497.
- (7) Zhang, J.; Li, Y.; Zhang, B.; Wang, H.; Xin, Q.; Song, A. Flexible indium–gallium–zinc–oxide Schottky diode operating beyond 2.45 GHz. *Nature communications* **2015**, *6* (1), 7561.
- (8) Georgiadou, D. G.; Semple, J.; Sagade, A. A.; Forstén, H.; Rantakari, P.; Lin, Y.-H.; Alkhalil, F.; Seitkhan, A.; Loganathan, K.; Faber, H. 100 GHz zinc oxide Schottky diodes processed from solution on a wafer scale. *Nature Electronics* **2020**, *3* (11), 718-725. Zhang, J.; Wang, H.; Wilson, J.; Ma, X.; Jin, J.; Song, A. Room temperature processed ultrahigh-frequency indium-gallium–zinc-oxide Schottky diode. *IEEE Electron Device Letters* **2016**, *37* (4), 389-392.
- (9) Sata, Y.; Moriya, R.; Morikawa, S.; Yabuki, N.; Masubuchi, S.; Machida, T. Electric field modulation of Schottky barrier height in graphene/MoSe₂ van der Waals heterointerface. *Applied Physics Letters* **2015**, *107* (2).
- (10) Di Bartolomeo, A. Graphene Schottky diodes: An experimental review of the rectifying graphene/semiconductor heterojunction. *Physics Reports* **2016**, *606*, 1-58.
- (11) Chen, C.-C.; Aykol, M.; Chang, C.-C.; Levi, A.; Cronin, S. B. Graphene-silicon Schottky diodes. *Nano letters* **2011**, *11* (5), 1863-1867. Sinha, D.; Lee, J. U. Ideal graphene/silicon Schottky junction diodes. *Nano letters* **2014**, *14* (8), 4660-4664.
- (12) Liu, Y.; Guo, J.; Zhu, E.; Liao, L.; Lee, S.-J.; Ding, M.; Shakir, I.; Gambin, V.; Huang, Y.; Duan, X. Approaching the Schottky–Mott limit in van der Waals metal–semiconductor junctions. *Nature* **2018**, *557* (7707), 696-700. Park, S.; Schultz, T.; Shin, D.; Mutz, N.; Aljarb, A.; Kang, H. S.; Lee, C.-H.; Li, L.-J.; Xu, X.; Tung, V. The Schottky–Mott rule expanded for two-dimensional semiconductors: Influence of substrate dielectric screening. *ACS nano* **2021**, *15* (9), 14794-14803. Li, Z.; Zheng, Y.; Li, G.; Wang, H.; Zhu, W.; Wang, H.; Chen, Z.; Yuan, Y.; Zeng, X. C.; Wu, Y. Resolving Interface Barrier Deviation from the Schottky–Mott Rule: A Mitigation Strategy via Engineering MoS₂–Metal van der Waals Contact. *The Journal of Physical Chemistry Letters* **2023**, *14* (12), 2940-2949.
- (13) Huang, H.; Sheng, Y.; Zhou, Y.; Zhang, Q.; Hou, L.; Chen, T.; Chang, R.-J.; Warner, J. H. 2D-layer-dependent behavior in lateral Au/WS₂/graphene photodiode devices with optical modulation of Schottky barriers. *ACS Applied nano materials* **2018**, *1* (12), 6874-6881.

- (14) Shi, J.; Zhang, J.; Yang, L.; Qu, M.; Qi, D. C.; Zhang, K. H. Wide bandgap oxide semiconductors: from materials physics to optoelectronic devices. *Advanced materials* **2021**, *33* (50), 2006230. Kim, H. J.; Park, K.; Kim, H. J. High - performance vacuum - processed metal oxide thin - film transistors: a review of recent developments. *Journal of the Society for Information Display* **2020**, *28* (7), 591-622.
- (15) Léonard, F.; Tersoff, J. Role of Fermi-level pinning in nanotube Schottky diodes. *Physical Review Letters* **2000**, *84* (20), 4693.
- (16) Mott, N. F.; Davis, E. A. *Electronic processes in non-crystalline materials*; OUP Oxford, 2012.
- (17) Chun, W.-J.; Ishikawa, A.; Fujisawa, H.; Takata, T.; Kondo, J. N.; Hara, M.; Kawai, M.; Matsumoto, Y.; Domen, K. Conduction and valence band positions of Ta₂O₅, TaON, and Ta₃N₅ by UPS and electrochemical methods. *The Journal of Physical Chemistry B* **2003**, *107* (8), 1798-1803.
- (18) Polyakov, A.; Smirnov, N.; Kozhukhova, E.; Vdovin, V.; Ip, K.; Heo, Y.; Norton, D.; Pearton, S. Electrical characteristics of Au and Ag Schottky contacts on n-ZnO. *Applied physics letters* **2003**, *83* (8), 1575-1577.
- (19) Brillson, L. J.; Lu, Y. ZnO Schottky barriers and Ohmic contacts. *Journal of Applied Physics* **2011**, *109* (12).
- (20) Gritsenko, V. A.; Perevalov, T. V.; Voronkovskii, V. A.; Gismatulin, A. A.; Kruchinin, V. N.; Aliev, V. S.; Pustovarov, V. A.; Prosvirin, I. P.; Roizin, Y. Charge transport and the nature of traps in oxygen deficient tantalum oxide. *ACS applied materials & interfaces* **2018**, *10* (4), 3769-3775.
- (21) Yoon, S.; Kim, H.; Kim, M.; Lee, H.; Yoon, D. Effect of substrate temperature on surface roughness and optical properties of Ta₂O₅ using ion-beam sputtering. *Thin Solid Films* **2005**, *475* (1-2), 239-242. Lu, Y.; Hwang, W.-S.; Yang, J. Effects of substrate temperature on the resistivity of non-stoichiometric sputtered NiO_x films. *Surface and Coatings Technology* **2002**, *155* (2-3), 231-235.
- (22) Park, G.-S.; Kim, Y. B.; Park, S. Y.; Li, X. S.; Heo, S.; Lee, M.-J.; Chang, M.; Kwon, J. H.; Kim, M.; Chung, U.-I. In situ observation of filamentary conducting channels in an asymmetric Ta₂O₅-x/TaO₂-x bilayer structure. *Nature communications* **2013**, *4* (1), 2382. Lee, S. H.; Moon, J.; Jeong, Y.; Lee, J.; Li, X.; Wu, H.; Lu, W. D. Quantitative, dynamic TaO_x memristor/resistive random access memory model. *ACS Applied Electronic Materials* **2020**, *2* (3), 701-709.
- (23) Kamble, V. B.; Umarji, A. M. Defect induced optical bandgap narrowing in undoped SnO₂ nanocrystals. *AIP Advances* **2013**, *3* (8).
- (24) Lampert, M. A. Simplified theory of space-charge-limited currents in an insulator with traps. *Physical Review* **1956**, *103* (6), 1648. Chen, A.; Zhang, W.; Dedon, L. R.; Chen, D.; Khatkhatay, F.; MacManus - Driscoll, J. L.; Wang, H.; Yarotski, D.; Chen, J.; Gao, X. Couplings of polarization with interfacial deep trap and Schottky interface controlled ferroelectric memristive switching. *Advanced Functional Materials* **2020**, *30* (43), 2000664.
- (25) Wang, Z.; Li, C.; Song, W.; Rao, M.; Belkin, D.; Li, Y.; Yan, P.; Jiang, H.; Lin, P.; Hu, M. Reinforcement learning with analogue memristor arrays. *Nature electronics* **2019**, *2* (3), 115-124.